analytical chemistry

pubs.acs.org/ac Article

Zinc-Based Metal–Organic Framework with MLCT Properties as an Efficient Electrochemiluminescence Probe for Trace Detection of Trenbolone

Xianzhen Song, Lu Zhao, Nuo Zhang, Lei Liu, Xiang Ren, Hongmin Ma, Chuannan Luo, Yuyang Li,* and Qin Wei*

Cite This: *Anal. Chem.* 2022, 94, 14054–14060 Read Online

ACCESS | Metrics & More | Article Recommendations | Supporting Information

ABSTRACT: In this work, we utilized polycyclic aromatic hydrocarbon (PAH) derivatives as ligands to develop a zinc-based metal–organic framework (Zn-MOF) as an effective detection probe to construct an electrochemiluminescence (ECL) sensor for trenbolone detection. As traditional ECL emitters, PAHs and their derivatives have limited luminescence efficiency because of the aggregation-induced quenching (ACQ) effect. Therefore, Zn-PTC was designed by the coordination of 3,4,9,10-perylenetetracarboxylic (PTC) in the MOF to eliminate the ACQ effect. Meanwhile, Zn-PTC formed based on an aromatic ligand possessed the metal-to-ligand charge-transfer (MLCT) effect, which could transfer the energy of Zn^{2+} to the aromatic ligand for strong luminescence. The ECL efficiency of Zn-PTC was calculated to be approximately 2.2 times that of the ligand (K_4PTC). Second, the Ag@Fe core–shell bimetallic nanocrystal was prepared for efficient activation of persulfate ($S_2O_8^{2-}$), thereby generating more sulfate radicals ($SO_4^{\bullet-}$) to further promote ECL emission. According to ECL characterizations, UV–vis and fluorescence spectra, and density functional theory calculations, the luminescence and signal amplification mechanisms were investigated. In addition, NKFRGKYKC (NKF) was introduced as an affinity ligand to directionally immobilize the target antibodies, thus releasing specific sites in their Fab fragment to enhance binding activity. Based on the above strategies, the constructed biosensor exhibited high sensitivity, realizing trace detection of TBE with a wide detection range (10 fg/mL–100 ng/mL) and a low detection limit (3.28 fg/mL). This study provided an important reference for sensitive monitoring of steroid pollutants in the environment.

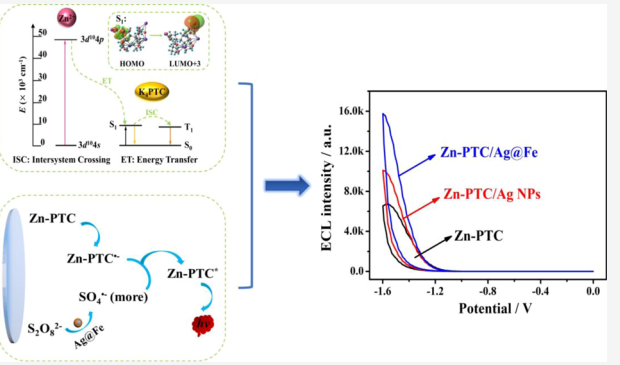

Downloaded via TSINGHUA UNIV on November 5, 2022 at 11:08:13 (UTC).
See https://pubs.acs.org/sharingguidelines for options on how to legitimately share published articles.

INTRODUCTION

Trenbolone (TBE) is a steroid used in fitness and animal husbandry.[1−3] At present, the metabolic emissions generated by its extensive use have triggered environmental pollution, especially natural water pollution, which has caused damage to human endocrine and nervous systems.[4−7] Hence, it is necessary to develop an effective method for TBE monitoring in natural water. Electrochemiluminescence (ECL) combines the advantages of electrochemistry and chemiluminescence, such as high sensitivity, simple test instruments, and low background signals, which is widely used in environmental monitoring.[8−12]

The metal–organic framework (MOF) is a porous material with special topological and designable pore structures, which is widely used in ECL sensing analysis.[13−17] As traditional ECL emitters, polycyclic aromatic hydrocarbons (PAHs) and their derivatives have received great attention due to their high quantum yield and good optoelectronic characteristics.[18,19] However, they will induce an aggregation-induced quenching (ACQ) effect, resulting in limited ECL efficiency.[20−22] Encouragingly, PAHs and their derivatives as ligands can eliminate the ACQ effect caused by $\pi-\pi$ stacking through their coordination in the MOF. At the same time, the designed MOF has the metal-to-ligand charge-transfer (MLCT) peculiarity, which can transfer the energy of metal ions from their outermost molecular orbital to the lowest unoccupied molecular orbital (LUMO) of ligands, thus achieving stable and efficient luminescence.[23,24] Among PAH derivatives, 3,4,9,10-perylene tetracarboxylic (PTC) can be used as an ideal ligand for the assembly of a luminescent MOF due to the high specific surface area, excellent conductivity, and stable ECL properties of persulfate ($S_2O_8^{2-}$).[25−27]

Received: August 18, 2022
Accepted: September 19, 2022
Published: September 29, 2022

© 2022 American Chemical Society

https://doi.org/10.1021/acs.analchem.2c03615
Anal. Chem. 2022, 94, 14054–14060

Scheme 1. Diagram of the Sensor Construction Process

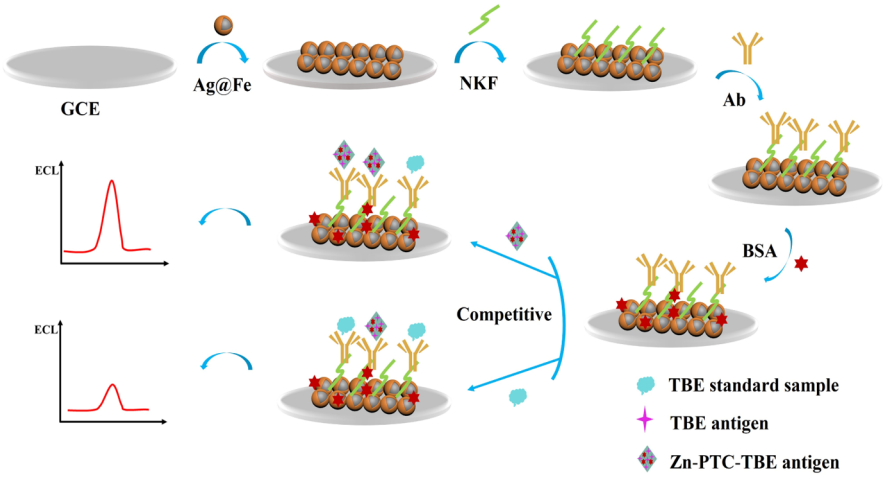

As we all know, a strong ECL signal is a guarantee for trace detection sensitivity.[28] However, the traditional signal amplification strategies are limited by the concentration of luminophores and co-reactants, resulting in unsatisfactory results. Therefore, an efficient ternary ECL system containing co-reaction promoters has been developed, which can achieve signal amplification by catalyzing the activation of the co-reactants.[28−30] In the reported literature,[31] silver has the best activation effect on $S_2O_8^{2-}$, which greatly accelerates the generation of the sulfate radical ($SO_4^{\bullet-}$), thereby promoting ECL emission. In addition, compared with the single catalytic mechanism of silver, the polymetallic complexes have higher catalytic activity for $S_2O_8^{2-}$.[32] In particular, iron also has a good catalytic effect on $S_2O_8^{2-}$.[31] Therefore, the Ag−Fe bimetallic nanocrystal could achieve more efficient signal amplification through the synergistic catalysis of silver and iron.

In this work, we developed an efficient sensing platform to realize TBE trace detection. PTC with ECL properties was used as an organic ligand to prepare Zn-PTC by its coordination fixation in the MOF. Meanwhile, Zn-PTC with an MLCT effect could achieve the energy transfer from the 3d molecular orbital of Zn^{2+} to the LUMO+3 of the K_4PTC singlet state. Therefore, Zn-PTC exhibited high ECL efficiency. In addition, the inherent porous structure of Zn-PTC made it have more binding sites, which made it an ideal detection probe. To improve the detection sensitivity, Ag@Fe bimetallic core−shell nanoparticles (NPs) were prepared as co-reaction promoters to accelerate the ECL process, thus enhancing the luminescence signal of Zn-PTC. Briefly, Ag@Fe NPs acted on co-reactants to promote the generation of active intermediates and then reacted with the free radicals of Zn-PTC (Zn-PTC$^{\bullet-}$) to produce more excited luminophores (Zn-PTC*). Meanwhile, the unique core−shell structure of Ag@Fe NPs realized the synergistic catalysis of different components. In addition, we introduced a small peptide affinity ligand (NKFRGKYKC, NKF) for the targeted immobilization of the TBE antibodies, so as to protect their binding activity, which further improved the detection sensitivity. According to the above advantages, the developed biosensor performed TBE detection in the range of 10 fg/mL to 100 ng/mL, and the detection limit was 3.28 fg/mL. This study could provide an efficient platform for dynamic trace monitoring of steroid pollutants produced by human metabolism and industrial emissions.

EXPERIMENTAL SECTION

Preparation of Zn-PTC. Zn-PTC was synthesized according to the reported literature with minor modifications.[33] First, 1 mmol of 3,4,9,10-perylenetetracarboxylic dianhydride (PTCDA) and 5 mmol of KOH were dispersed in 5 mL of ultrapure water and then stirred at 55 °C for 12 h. Subsequently, 30 mL of ethanol was added to obtain K_4PTC. Next, the prepared K_4PTC (0.05 mmol) was mixed in 15 mL of $Zn(CH3COO)_2$ solution (7 mM) and stirred for 0.5 h. Finally, the mixed solution was heated at 100 °C for 12 h. After washing three times with ultrapure water, Zn-PTC was collected by centrifugation (9000 rpm).

Preparation of Ag@Fe Bimetallic NPs. First, 200 mL of $FeSO_4{\cdot}7H_2O$ solution was prepared (4.6 mM); then, sodium citrate (0.46 mM) was added as the surfactant. Subsequently, 4.6 mM of $AgNO_3$ was added with stirring for 0.5 h. After that, sodium borohydride ($NaBH_4$, 8.8 mM) was added as a reducing agent, and the mixture was stirred for 10 min. Correspondingly, the solution color changed from transparent to black. Finally, Ag@Fe NPs were acquired by magnetic separation and washing with ultrapure water three times.

Preparation of Zn-PTC-TBE Detection Probes. The aminated Zn-PTC (the amination process was described in the Supporting Information) was dispersed in 2 mL of phosphate buffered saline (PBS); then, 200 μL of glutaraldehyde and 100 μL of TBE antigen were added successively for cross-linking. Finally, 10 μL of bovine serum albumin (BSA) was added.

Construction of the Biosensor. First, the bare glassy carbon electrode (GCE) was polished, and then, 10 μL of Ag@Fe was modified on the treated electrode. Subsequently, 6 μL of NKF was modified on the electrode. Next, 10 μL of TBE antibody (Ab) and 3 μL of BSA were added in turn. Finally, 6 μL of TBE standard samples and 10 μL of Zn-PTC-TBE probes were sequentially dropped on the modified electrode to construct the competitive biosensor. The detailed construction procedure of the sensor was exhibited in Scheme 1.

Measurement Conditions. In this work, the test solution is $K_2S_2O_8$ dissolved in PBS (80 mM, pH = 7.0). Parameter settings: the voltage range is −1.6−0 V, the high voltage is 800 V, and the scanning speed is 0.1 V/s.

https://doi.org/10.1021/acs.analchem.2c03615
Anal. Chem. 2022, 94, 14054−14060

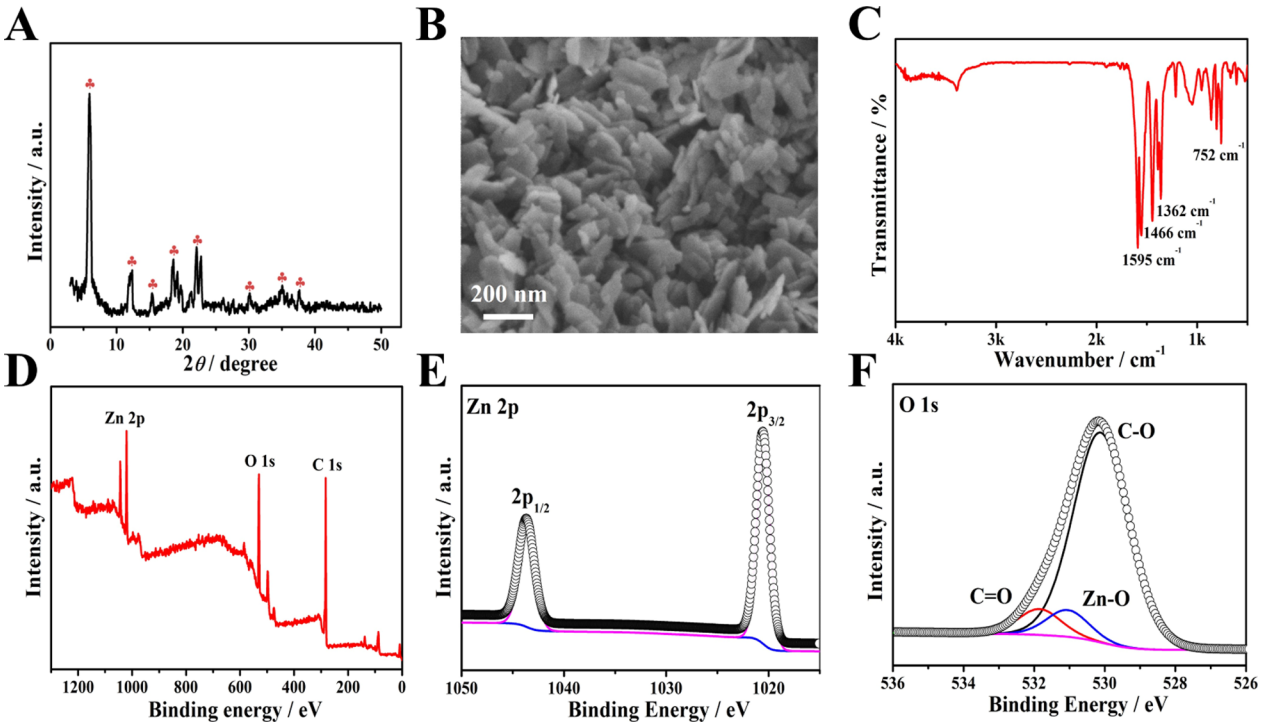

Figure 1. (A) XRD pattern, (B) scanning electron microscopy image, (C) FT-IR spectrum, and (D−F) XPS spectra of Zn-PTC.

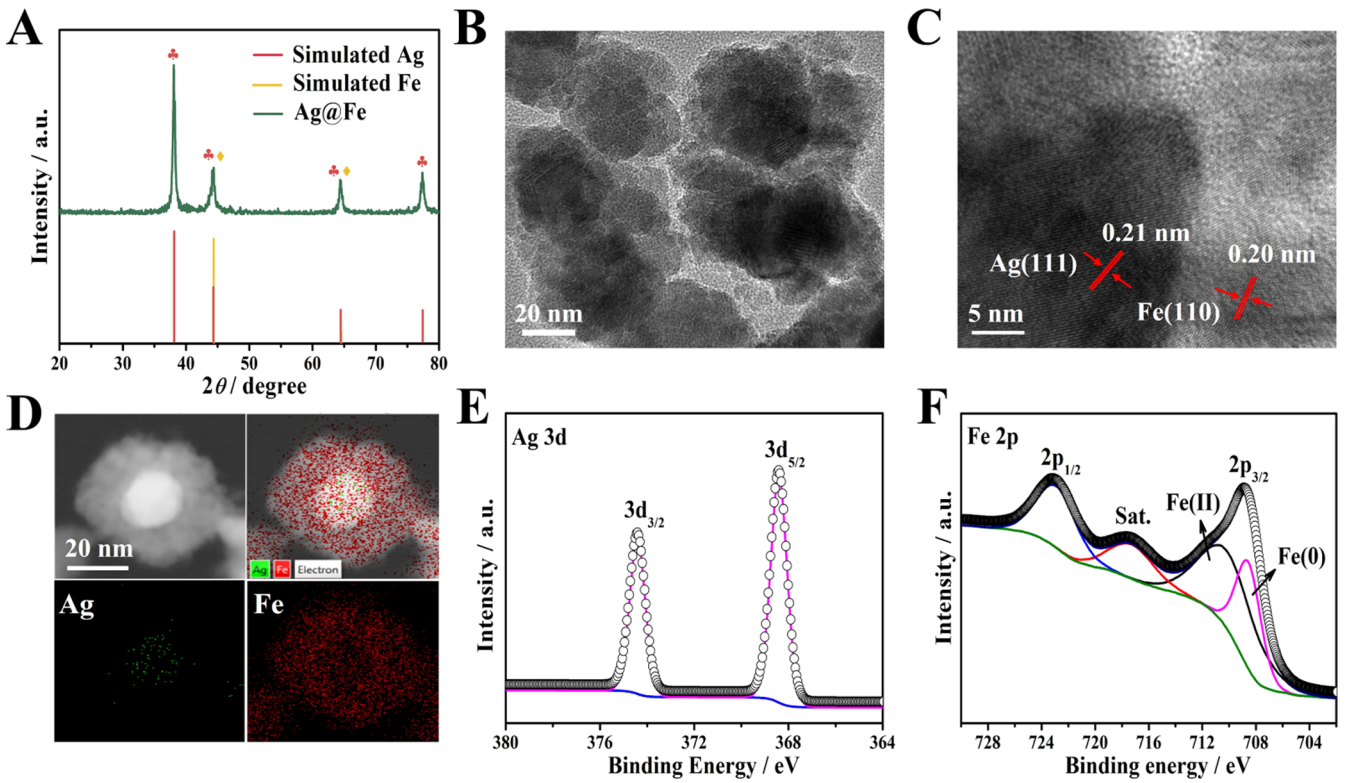

Figure 2. (A) XRD pattern, (B−D) TEM, HRTEM, and elemental mapping images, and (E−F) XPS spectra of Ag@Fe.

RESULTS AND DISCUSSION

Characterization of Zn-PTC. In Figure 1A, the X-ray diffraction (XRD) pattern of Zn-PTC exhibited several diffraction peaks, which matched the previous studies.[33] In Figure 1B, Zn-PTC presented the shape of nanosheets with a size of about 200 nm. In the FT-IR spectrum of Zn-PTC (Figure 1C), the two peaks at 1595 and 752 cm^{-1} corresponded to the skeleton vibration of the aromatic ring and $\delta_{=C-H}$, which verified the existence of aromatics.[27,34] At the same time, the other peaks at 1362 and 1466 cm^{-1} were attributed to ν_{COO^-}, confirming the coordination of Zn^{2+}.[33] Figure 1D−F showed the X-ray photoelectron spectroscopy (XPS) spectra of Zn-PTC, and all elements of Zn, C,

https://doi.org/10.1021/acs.analchem.2c03615
Anal. Chem. 2022, 94, 14054−14060

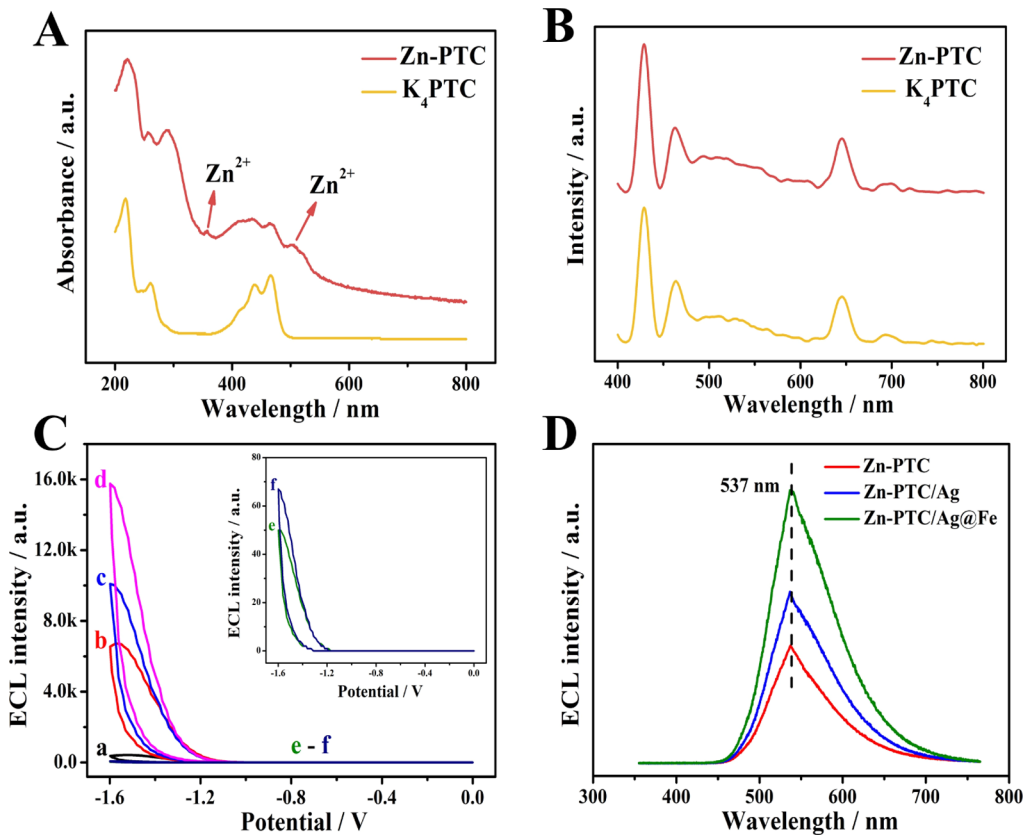

Figure 3. (A) UV−vis and (B) FL spectra of Zn-PTC and K_4PTC. (C) ECL-potential curves of (a) GCE, (b) Zn-PTC/GCE, (c) Zn-PTC/Ag NPs/GCE, and (d) Zn-PTC/Ag@Fe/GCE in $S_2O_8^{2-}$ (80 mM, pH = 7.0) and (e) Zn-PTC/GCE and (f) Zn-PTC/Ag@Fe/GCE in PBS. (D) ECL spectra of Zn-PTC/GCE, Zn-PTC/Ag NPs/GCE, and Zn-PTC/Ag@Fe/GCE in $S_2O_8^{2-}$ (80 mM, pH = 7.0).

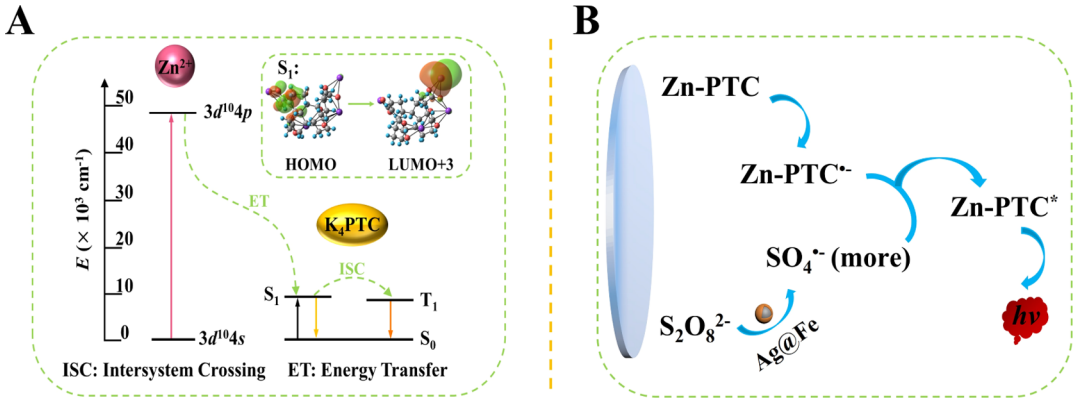

Figure 4. (A) Energy transfer process model from Zn^{2+} to K_4PTC (inset: HOMO and LUMO of S_1 of K_4PTC). (B) ECL mechanism diagram of the Zn-PTC/Ag@Fe/$S_2O_8^{2-}$ system.

and O in it were observed. In addition, the two peaks at 1043.6 and 1020.5 eV in the Zn 2p region belonged to Zn^{2+} $2p_{1/2}$ and Zn^{2+} $2p_{3/2}$, respectively.[35] Meanwhile, the three peaks at 531.8, 531.1, and 530.1 eV in the O 1s region corresponded to C═O, Zn−O, and C−O, which further verified the successful coordination of Zn^{2+}.[36] The above results indicated the successful synthesis of Zn-PTC.

Characterization of Ag@Fe Bimetallic NPs. In Figure 2A, the XRD diffraction peaks of Ag@Fe were indexed to the (111), (200), (220), and (311) crystal planes of Ag NPs (JCPDS 87-0717) and the (110) and (200) crystal planes of Fe NPs (JCPDS 85-1410). According to the transmission electron microscopy (TEM) images, we observed that Ag@Fe presented a core−shell nanosphere structure with a diameter of 50 nm. Meanwhile, Ag@Fe had clear lattices, and the lattice spacings of 0.21 and 0.20 nm were sequentially matched with the Ag(111) and Fe(110) crystal planes, indicating that Ag was the core and Fe was the shell (Figure 2B,C). In Figure 2D, the elemental mapping analysis results further confirmed the above structure. The full XPS spectrum of Ag@Fe exhibited obvious peaks of Ag 3d and Fe 2p (Figure S1). In Figure 2E, the two distinct peaks at 374.4 and 368.4 eV were assigned to Ag $3d_{3/2}$ and Ag $3d_{5/2}$, respectively.[11] In Figure 2F, the two peaks at 710.5 and 708.9 eV belonged to Fe $2p_{3/2}$, representing Fe(II) and Fe(0), respectively. Furthermore, the peaks at 722.6 and 717.1 eV were attributed to Fe $2p_{1/2}$ and a satellite peak.[37]

https://doi.org/10.1021/acs.analchem.2c03615
Anal. Chem. 2022, 94, 14054−14060

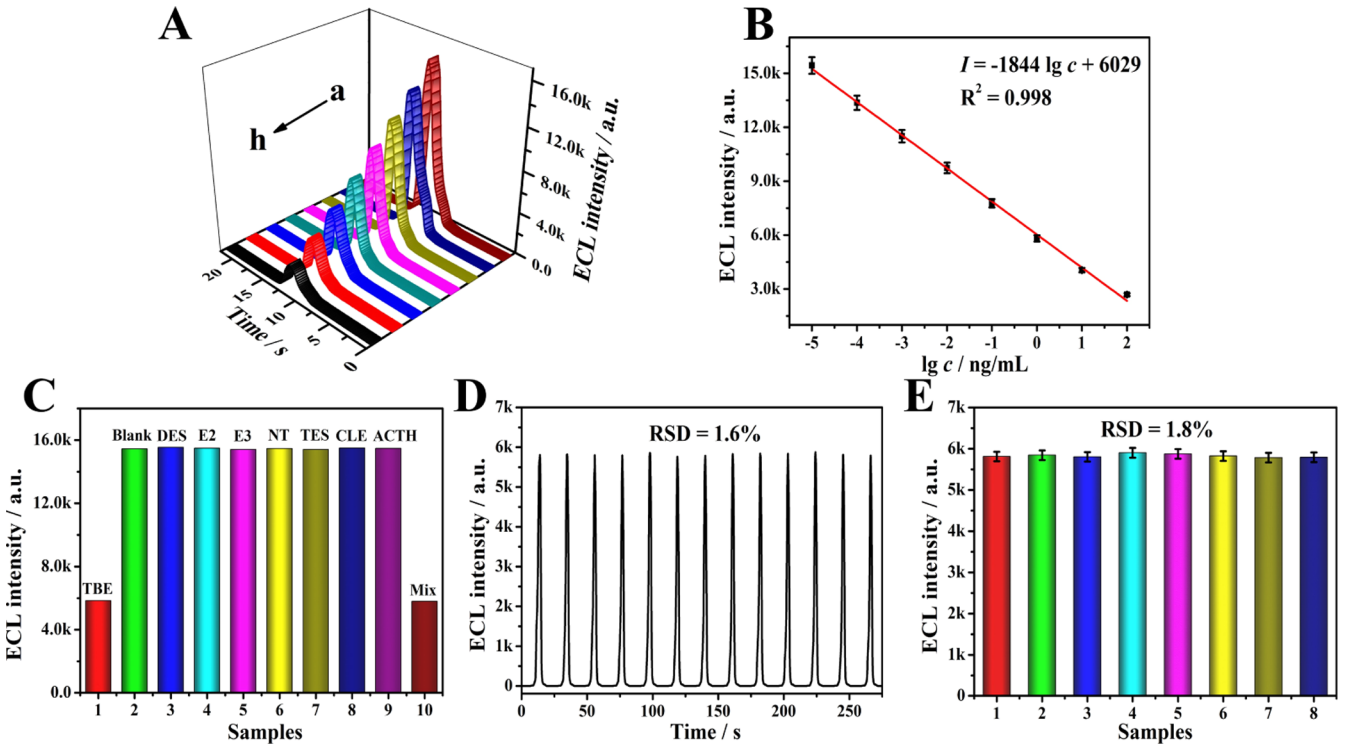

Figure 5. (A) ECL−time curves of the biosensor under different TBE standard sample concentrations (a−h: 10 fg/mL−100 ng/mL). (B) Correlation calibration curve. (C) Selectivity, (D) stability, and (E) reproducibility of the biosensor.

Luminescence Mechanism of Zn-PTC. The luminescence mechanism was researched through UV−vis and fluorescence (FL) spectra and density functional theory (DFT) calculations. In Figure 3A, compared with the K_4PTC ligand, the UV−vis spectrum of Zn-PTC presented two new characteristic absorption peaks at 356 and 504 nm, which were attributed to Zn^{2+}. Meanwhile, the absorption peak of K_4PTC at 261 nm was divided into two peaks at 257 and 288 nm, proving the successful coordination of K_4PTC with the Zn(II) center.[11] Furthermore, the main FL emission bands of Zn-PTC at 428, 462, 645, and 693 nm were identified with those of K_4PTC (Figure 3B), which confirmed that the luminescent center of Zn-PTC was located on the ligands. At the same time, we could also conclude that Zn-PTC had the MLCT effect, which was verified by DFT calculations. Specifically, the energy levels of K_4PTC were calculated using the Gaussian09 program by the B3LYP/GENECP method and the 6−31 G*/LANL2DZ basis set. The detailed energy transfer process model from Zn^{2+} to K_4PTC is shown in Figure 4A. First, K_4PTC had energy transmission after excitating to its singlet state (S_1) from the ground state (S_0) with an excitation energy of 9517 cm^{-1}. On the other hand, the energy was transferred from the $3d^{10}4p$ vibrational level of Zn^{2+} to the LUMO+3 of S_1. Finally, the electron of S_1 was transferred to the triplet first excited state (T_1); then, K_4PTC emitted strong luminescence and returned to S_0.

ECL Mechanism of the Zn-PTC/Ag@Fe/$S_2O_8^{2-}$ System. Herein, we explored the signal amplification mechanism of this system by testing the ECL signals of different modified electrodes. In Figure 3C, GCE showed a weak ECL signal (curve *a*). When Zn-PTC was modified on GCE as an emitter, a distinct ECL emission was observed (curve *b*). After Ag@Fe NPs were continued to be modified, the ECL signal was greatly enhanced, which was attributed to their efficient catalysis for $S_2O_8^{2-}$ (curve *d*). At the same time, the signal amplification effect of Ag NPs on Zn-PTC was tested, and the results showed that the ECL response of Zn-PTC/Ag NPs/GCE was significantly lower than that of Zn-PTC/Ag@Fe/GCE, confirming the superiority of the synergistic catalysis mechanism (curve *c*). In addition, the ECL signals of Zn-PTC/GCE (curve *e*) and Zn-PTC/Ag@Fe/GCE (curve *f*) in PBS were tested, and neither of them produced ECL responses. Hence, it could be concluded that Ag@Fe NPs could not promote ECL emission of Zn-PTC in the absence of $S_2O_8^{2-}$. In Figure 3D, the corresponding ECL signals increased sequentially after the modifications of Ag NPs and Ag@Fe NPs on Zn-PTC/GCE. Meanwhile, the ECL emission peak position remained unchanged (537 nm), and the peak shape was consistent. Therefore, the ECL spectrum results indicated that Ag@Fe NPs did not act on Zn-PTC, which further confirmed the above inferences.

The specific ECL mechanism is shown in Figure 4B. First, Zn-PTC gained electrons to generate active species (Zn-$PTC^{\bullet -}$), and Ag@Fe catalyzed the reduction of $S_2O_8^{2-}$ to produce more $SO_4^{\bullet -}$. Subsequently, the obtained Zn-$PTC^{\bullet -}$ reacted with $SO_4^{\bullet -}$ to obtain Zn-PTC*. Finally, Zn-PTC* relaxed back to the ground state and produced luminescence. The mechanism formulae were as follows

$$Zn - PTC + e^- \rightarrow Zn - PTC^{\bullet -} \quad (1)$$

$$S_2O_8^{2-} + e^- \rightarrow SO_4^{2-} + SO_4^{\bullet -}(\text{more, promoted by Ag@Fe}) \quad (2)$$

$$Zn - PTC^{\bullet -} + SO_4^{\bullet -} \rightarrow Zn - PTC^* + SO_4^{2-} \quad (3)$$

$$Zn - PTC^* \rightarrow Zn - PTC + h\nu \quad (4)$$

https://doi.org/10.1021/acs.analchem.2c03615
Anal. Chem. 2022, 94, 14054−14060

ECL Efficiency of Zn-PTC and K_4PTC. In this study, we calculated the ECL efficiency of Zn-PTC and K_4PTC with the $[Ru(bpy)_3]^{2+}$/(TBA)BF_4 system as a reference. The calculation equation is shown below[38,39]

$$\Phi_{ECL} = \Phi^{\circ}_{ECL}(Q_f^{\circ}/I^{\circ}Q_f) \quad (5)$$

Herein, Φ°ECL refers to the ECL efficiency of the reference system. Specifically, Φ°ECL is the ECL efficiency of 1 mM $[Ru(bpy)_3]^{2+}$ in (TBA)BF_4 solution. I and I° represent the ECL intensities of the investigated species and $[Ru(bpy)_3]^{2+}$. Q_f and Q°f represent the faradaic charges delivered by the corresponding species. After calculation, the ECL efficiency of K_4PTC and Zn-PTC was 4.5 and 10.2%. The results exhibited that the ECL efficiency of K_4PTC was much lower than that of Zn-PTC, which was attributed to the elimination of the ACQ effect. In addition, the ECL efficiency of Zn-PTC/$S_2O_8^{2-}$ was also better than other systems (the detailed results are shown in Table S1).

TBE Detection Performance. The ECL responses of different TBE standard sample concentrations were tested under optimal conditions. In Figure 5A, we observed that the ECL responses gradually decreased with the increase in TBE standard sample concentrations. In addition, the ECL signals were linearly related to the concentrations of TBE standard samples, and the linear equation was $I = -1844 \lg c + 6029$ (I: ECL intensity, c: TBE standard sample concentration, Figure 5B). Based on the above results, we inferred that the constructed biosensor could achieve trace detection of TBE in the linear range of 10 fg/mL−100 ng/mL with a detection limit of 3.28 fg/mL. Compared with other platforms, the proposed biosensor showed higher TBE detection efficiency (the detailed results are shown in Table S2).

In addition, we tested the selectivity, stability, and reproducibility of the proposed biosensor. First, several similar environmental pollutants were selected (diethylstilbestrol, estradiol, estriol, nortestosterone, testosterone, clenbuterol, and adreno cortico tropic hormone) as interferences to investigate the selectivity of the sensor. In Figure 5C, the ECL signals of the interferences were similar to those of the blank sample, which were much higher than TBE. Furthermore, the ECL signal of TBE was consistent with that of the mixed samples (1 ng/mL TBE +8 ng/mL interferences). The results exhibited that the developed biosensor possessed good selectivity. In Figure 5D, we observed that the ECL signals from several cycle scans were nearly identical, and the corresponding relative standard deviation (RSD) was 1.6%, indicating good stability of the sensor. Finally, we tested the ECL responses of eight different modified electrodes, and the results exhibited little signal deviation, with an RSD of 1.8%, which confirmed that the developed biosensor had good reproducibility.

Natural Water Sample Analysis. We randomly selected three river water samples for TBE detection to verify the practical application ability of the developed biosensor. Taking the selected river water as the initial sample, the detection recovery and RSD of the sensor were studied by the standard addition recovery method. In Table S3, the calculated recovery and RSD were 97.4−102.3% and 1.6−2.6%, suggesting that the developed biosensor with good accuracy and precision was suitable for trace detection of steroid pollutants.

CONCLUSIONS

In conclusion, an efficient ECL-sensing platform for environmental monitoring was developed. First, Zn-PTC was prepared based on the coordination of PTC in the MOF, thus eliminating the ACQ effect. Moreover, the prepared Zn-PTC possessed the MLCT effect, which enhanced the luminescence by transferring the energy of Zn^{2+} from the outermost molecular orbital to the LUMO+3 of K_4PTC. Hence, Zn-PTC with high ECL efficiency was developed as a trace detection probe. Second, the Ag@Fe bimetallic nanocrystal was prepared as a co-reaction promoter, whose special core−shell structure and inherent synergistic catalytic mechanism realized the efficient activation of $S_2O_8^{2-}$, thereby generating more $SO_4^{\bullet-}$ to promote ECL emission. Convincingly, the luminescence and signal amplification mechanisms were verified by UV−vis and FL spectra, ECL tests, and DFT calculations. Finally, NKF was introduced as an affinity ligand to protect the binding activity of the target antibodies, thereby improving the detection sensitivity. Based on this, the proposed biosensor exhibited high precision and accuracy in natural water detection, which provided an effective method for dynamic trace monitoring of environmental pollutants.

ASSOCIATED CONTENT

Supporting Information

The Supporting Information is available free of charge at https://pubs.acs.org/doi/10.1021/acs.analchem.2c03615.

Materials, apparatus, amination of Zn-PTC, XPS spectrum of Ag@Fe NPs, electrochemical behavior of the sensor, condition optimization, comparison of ECL efficiency, comparison with other methods, and natural water sample analysis (PDF)

AUTHOR INFORMATION

Corresponding Authors

Yuyang Li − *Collaborative Innovation Center for Green Chemical Manufacturing and Accurate Detection, Key Laboratory of Interfacial Reaction & Sensing Analysis in Universities of Shandong, School of Chemistry and Chemical Engineering, University of Jinan, Jinan 250022 Shandong, China*; orcid.org/0000-0002-1399-9381; Phone: +86 531 82765730; Email: chm_liyy@ujn.edu.cn; Fax: +86 531 82765969

Qin Wei − *Collaborative Innovation Center for Green Chemical Manufacturing and Accurate Detection, Key Laboratory of Interfacial Reaction & Sensing Analysis in Universities of Shandong, School of Chemistry and Chemical Engineering, University of Jinan, Jinan 250022 Shandong, China*; orcid.org/0000-0002-3034-8046; Email: sdjndxwq@163.com

Authors

Xianzhen Song − *Collaborative Innovation Center for Green Chemical Manufacturing and Accurate Detection, Key Laboratory of Interfacial Reaction & Sensing Analysis in Universities of Shandong, School of Chemistry and Chemical Engineering, University of Jinan, Jinan 250022 Shandong, China*

Lu Zhao − *Collaborative Innovation Center for Green Chemical Manufacturing and Accurate Detection, Key Laboratory of Interfacial Reaction & Sensing Analysis in Universities of Shandong, School of Chemistry and Chemical*

Engineering, University of Jinan, Jinan 250022 Shandong, China

Nuo Zhang − *Collaborative Innovation Center for Green Chemical Manufacturing and Accurate Detection, Key Laboratory of Interfacial Reaction & Sensing Analysis in Universities of Shandong, School of Chemistry and Chemical Engineering, University of Jinan, Jinan 250022 Shandong, China*

Lei Liu − *Collaborative Innovation Center for Green Chemical Manufacturing and Accurate Detection, Key Laboratory of Interfacial Reaction & Sensing Analysis in Universities of Shandong, School of Chemistry and Chemical Engineering, University of Jinan, Jinan 250022 Shandong, China*

Xiang Ren − *Collaborative Innovation Center for Green Chemical Manufacturing and Accurate Detection, Key Laboratory of Interfacial Reaction & Sensing Analysis in Universities of Shandong, School of Chemistry and Chemical Engineering, University of Jinan, Jinan 250022 Shandong, China;* orcid.org/0000-0002-4321-4282

Hongmin Ma − *Collaborative Innovation Center for Green Chemical Manufacturing and Accurate Detection, Key Laboratory of Interfacial Reaction & Sensing Analysis in Universities of Shandong, School of Chemistry and Chemical Engineering, University of Jinan, Jinan 250022 Shandong, China;* orcid.org/0000-0002-7061-8944

Chuannan Luo − *Collaborative Innovation Center for Green Chemical Manufacturing and Accurate Detection, Key Laboratory of Interfacial Reaction & Sensing Analysis in Universities of Shandong, School of Chemistry and Chemical Engineering, University of Jinan, Jinan 250022 Shandong, China*

Complete contact information is available at: https://pubs.acs.org/10.1021/acs.analchem.2c03615

Notes

The authors declare no competing financial interest.

■ ACKNOWLEDGMENTS

This study was supported by the Special Foundation for Taishan Scholar Professorship of Shandong Province (no. ts20130937), the National Natural Science Foundation of China (nos. 21777056, 51904114), the Natural Science Foundation for Young of Shandong Province (nos. ZR2020QB097, ZR201911110108), and the Innovation Team Project of Colleges and Universities in Jinan (no. 2019GXRC027).

■ REFERENCES

(1) Schiffer, B.; Daxenberger, A.; Meyer, K.; Meyer, H. H. *Environ. Health Perspect.* **2001**, *109*, 1145−1151.
(2) Borodi, G.; Turza, A.; Camarasan, P. A.; Ulici, A. *J. Mol. Struct.* **2020**, *1212*, 128127.
(3) Richold, M. *Arch. Toxicol.* **1988**, *61*, 249−258.
(4) Zhang, Y.; Snow, D. D.; Bartelt-Hunt, S. L. *Environ. Sci. Technol.* **2016**, *50*, 13256−13264.
(5) Khetan, S. K.; Collins, T. J. *Chem. Rev.* **2007**, *107*, 2319−2364.
(6) Kolodziej, E. P.; Qu, S.; Forsgren, K. L.; Long, S. A.; Gloer, J. B.; Jones, G. D.; Schlenk, D.; Baltrusaitis, J.; Cwiertny, D. M. *Environ. Sci. Technol.* **2013**, *47*, 5031−5041.
(7) Zhang, S. Z.; Jiao, Z. H.; Zhao, X.; Sun, M. Z.; Feng, X. Z. *Environ. Pollut.* **2021**, *289*, 117710.
(8) Li, L. L.; Chen, Y.; Zhu, J. J. *Anal. Chem.* **2017**, *89*, 358−371.
(9) Hu, L. Z.; Xu, G. B. *Chem. Soc. Rev.* **2010**, *39*, 3275−3304.
(10) Babamiri, B.; Salimi, A.; Hallaj, R. *Biosens. Bioelectron.* **2018**, *102*, 328−335.
(11) Zhao, L.; Wang, X. Z.; Song, H.; Liu, X. Y.; Ju, D.; Ai, Q.; Wei, H. X.; Wu, D. *Chem. Eng. J.* **2022**, *434*, 134691.
(12) Chen, H. M.; Zhang, H.; Yuan, R.; Chen, S. H. *Anal. Chem.* **2017**, *89*, 2823−2829.
(13) Kent, C. A.; Liu, D. M.; Meyer, T. J.; Lin, W. B. *J. Am. Chem. Soc.* **2012**, *134*, 3991−3994.
(14) Wang, C.; Lin, W. B. *J. Am. Chem. Soc.* **2011**, *133*, 4232−4235.
(15) Song, X. Z.; Zhao, L.; Luo, C. N.; Ren, X.; Yang, L.; Wei, Q. *Anal. Chem.* **2021**, *93*, 9704−9710.
(16) Zhao, L.; Song, X. Z.; Ren, X.; Wang, H.; Fan, D. W.; Wu, D.; Wei, Q. *Biosens. Bioelectron.* **2021**, *191*, 113409.
(17) Zhao, L.; Song, X. Z.; Ren, X.; Fan, D. W.; Wei, Q.; Wu, D. *Anal. Chem.* **2021**, *93*, 8613−8621.
(18) Liu, J. L.; Tang, Z. L.; Zhang, J. Q.; Chai, Y. Q.; Zhuo, Y.; Yuan, R. *Anal. Chem.* **2018**, *90*, 5298−5305.
(19) Huang, Y. J.; Xing, J.; Gong, Q. Y.; Chen, L. C.; Liu, G. F.; Yao, C. J.; Wang, Z. R.; Zhang, H. L.; Chen, Z.; Zhang, Q. C. *Nat. Commun.* **2019**, *10*, 169.
(20) Hong, Y. N.; Lam, J. W. Y.; Tang, B. Z. *Chem. Soc. Rev.* **2011**, *40*, 5361−5388.
(21) Zhao, Z. J.; Lu, P.; Lam, J. W. Y.; Wang, Z. M.; Chan, C. Y. K.; Sung, H. H. Y.; Williams, I. D.; Ma, Y. G.; Tang, B. Z. *Chem. Sci.* **2011**, *2*, 672−675.
(22) Zhao, Z. J.; Chen, S. M.; Lam, J. W. Y.; Lu, P.; Zhong, Y. C.; Wong, K. S.; Kwok, H. S.; Tang, B. Z. *Chem. Commun.* **2010**, *46*, 2221−2223.
(23) Kobayashi, A.; Shimizu, K.; Watanabe, A.; Nagao, Y.; Yoshimura, N.; Yoshida, M.; Kato, M. *Inorg. Chem.* **2019**, *58*, 2413−2421.
(24) Maurer, L. A.; Pearce, O. M.; Maharaj, F. D. R.; Brown, N. L.; Amador, C. K.; Damrauer, N. H.; Marshak, M. P. *Inorg. Chem.* **2021**, *60*, 10137−10146.
(25) Zhao, M.; Liao, N.; Zhuo, Y.; Chai, Y. Q.; Wang, J. P.; Yuan, R. *Anal. Chem.* **2015**, *87*, 7602−7609.
(26) Song, X. Z.; Shao, X. R.; Dai, L.; Fan, D. W.; Ren, X.; Sun, X.; Luo, C. N.; Wei, Q. *ACS Appl. Mater. Interfaces* **2020**, *12*, 9098−9106.
(27) Zhang, H.; Zuo, F. M.; Tan, X. R.; Xu, S. H.; Yuan, R.; Chen, S. H. *Biosens. Bioelectron.* **2018**, *104*, 65−71.
(28) Lei, Y. M.; Wen, R. X.; Zhou, J.; Chai, Y. Q.; Yuan, R.; Zhuo, Y. *Anal. Chem.* **2018**, *90*, 6851−6858.
(29) Yu, Y. Q.; Zhang, H. Y.; Chai, Y. Q.; Yuan, R.; Zhuo, Y. *Biosens. Bioelectron.* **2016**, *85*, 8−15.
(30) Hu, L. Y.; Wu, Y.; Xu, M.; Gu, W. L.; Zhu, C. Z. *Chem. Commun.* **2020**, *56*, 10989−10999.
(31) Anipsitakis, G. P.; Dionysiou, D. D. *Environ. Sci. Technol.* **2004**, *38*, 3705−3712.
(32) Hu, L. Y.; Dong, T. T.; Zhao, K.; Deng, A. P.; Li, J. G. *Microchim. Acta* **2017**, *184*, 3415−3423.
(33) Wang, J. M.; Yao, L. Y.; Huang, W.; Yang, Y.; Liang, W. B.; Yuan, R.; Xiao, D. R. *ACS Appl. Mater. Interfaces* **2021**, *13*, 44079−44085.
(34) Fu, X. M.; Yang, Y.; Wang, N.; Chen, S. H. *Sens. Actuators, B* **2017**, *250*, 584−590.
(35) Li, C. H.; Yang, W. X.; Zhang, X. S.; Han, Y.; Tang, W. Z.; Yue, T. L.; Li, Z. H. *J. Mater. Chem. C* **2020**, *8*, 2054−2064.
(36) Zhang, Z. T.; Pfefferle, L.; Haller, G. L. *Chin. J. Catal.* **2014**, *35*, 856−863.
(37) Glaria, A.; Soulé, S.; Hallali, N.; Ojo, W. S.; Mirjolet, M.; Fuks, G.; Cornejo, A.; Allouche, J.; Dupin, J. C.; Martinez, H.; Carrey, J.; Chaudret, B.; Delpech, F.; Lachaize, S.; Nayral, C. *RSC Adv.* **2018**, *8*, 32146−32156.
(38) Dennany, L.; Hogan, C. F.; Keyes, T. E.; Forster, R. J. *Anal. Chem.* **2006**, *78*, 1412−1417.
(39) Peng, H. P.; Deng, H. H.; Jian, M. L.; Liu, A. L.; Bai, F. Q.; Lin, X. H.; Chen, W. *Microchim. Acta* **2017**, *184*, 735−743.